Effects of keels on ice bottom turbulence exchange

Eric D. Skyllingstad, Clayton A. Paulson, and W. Scott Pegau
College of Oceanic and Atmospheric Sciences, Oregon State University, Corvallis, Oregon, USA

Miles G. McPhee
McPhee Research Company, Naches, Washington, USA

Timothy Stanton
Naval Postgraduate School, Monterey, California, USA

Received 24 May 2002; revised 23 May 2003; accepted 11 September 2003; published 4 December 2003.

[1] The effects of ice keels on the upper ocean are examined using a combination of turbulence measurements and output from a large-eddy simulation (LES) model. Two cases are examined, one during the winter when the under-ice boundary layer is relatively deep (~20 m) and near the freezing point and a second during the summer when the ice is melting and the boundary layer consists of a shallow (~0.5 m), highly stratified fresh layer. In the winter case, measurements show that flow disruption by a 10-m-deep keel causes enhanced vertical mixing, increasing the heat flux from a background value of ~5 W m^{-2} to values averaging ~25 W m^{-2}. Simulations using the LES model are in good agreement with the measurements and indicate that the keel generates a turbulent wake region extending hundreds of meters downstream from the keel. Elevated heat fluxes in the wake region are generated by increased entrainment of warmer water from beneath the mixed layer. Simulations of summer cases demonstrate that shallow keels (~0.5 m) generate strong turbulence that is able to rapidly mix the fresh layer in the lee of keels. However, this effect decreases quickly as the fresh layer accelerates to match the ice velocity. Deeper keels (1 m) follow a similar pattern but generate more mixing as the fresh layer is forced under the keel. Simulated ice melt heat fluxes are similar to estimates made from ice balance measurements taken during the Surface Heat Budget of the Arctic Ocean summer field program. *INDEX TERMS:* 4540 Oceanography: Physical: Ice mechanics and air/sea/ice exchange processes; 4568 Oceanography: Physical: Turbulence, diffusion, and mixing processes; 4572 Oceanography: Physical: Upper ocean processes; 4544 Oceanography: Physical: Internal and inertial waves; *KEYWORDS:* keels, turbulence, sea ice, internal waves, ice-ocean exchange

Citation: Skyllingstad, E. D., C. A. Paulson, W. S. Pegau, M. G. McPhee, and T. Stanton, Effects of keels on ice bottom turbulence exchange, *J. Geophys. Res.*, *108*(C12), 3372, doi:10.1029/2002JC001488, 2003.

1. Introduction

[2] Defining the fluxes at the interface between sea ice and the upper ocean is crucial for accurate modeling of the polar ocean and its ice coverage. This is particularly true in the summer melt season when solar heating causes increased melting at lead edges and under the pack ice. Because leads do not reflect as much visible solar radiation as ice floes, an increase in lead fraction can cause more rapid ice melting during the summer. As ice coverage decreases, more solar radiation is absorbed, forming a nonlinear process known as the ice-albedo feedback. Ice coverage strongly affects the Earth's heat budget, so it is critical that we understand the processes that control ice formation and melting and the ice-albedo feedback.

[3] Turbulent transport of heat from the ocean to the ice/water interface is the main process in modeling ice melting. In particular, it is important to understand how turbulent heat flux varies between the edge of an ice floe and the ice bottom, as melting in these two regions can control the ice-albedo feedback. The work presented here addresses one component of this problem, namely, the role of ice bottom keels in generating turbulent mixing. This work is part of a much larger effort known as the Surface Heat Budget of the Arctic Ocean (SHEBA) experiment, which was designed in part to understand processes important for sea ice formation and melting.

[4] A specific goal of SHEBA was to develop a conceptual model of summer time ice behavior so that better representations of sea ice could be developed for coupled climate models. A key question during the summer melt period concerns the fate of fresh water produced as snow and sea ice melt. As melting progresses, fresh water tends to pool in leads and eventually under the ice pack. Unfortunately, direct measurements of temperature and salinity within ~1 m of the ice bottom were not taken during the summer SHEBA experiment because of equipment

0148-0227/03/2002JC001488$09.00

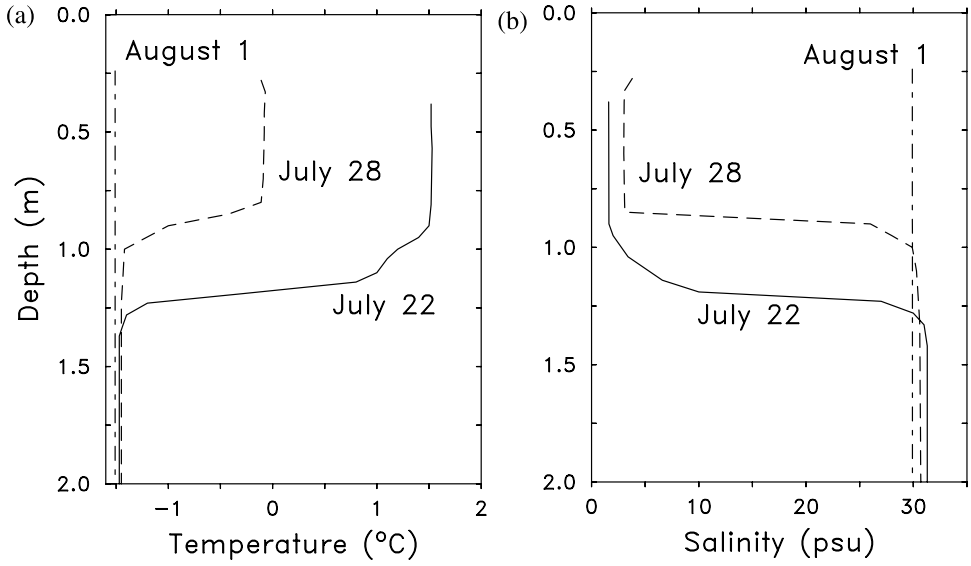

Figure 1. Vertical profiles of (a) temperature and (b) salinity taken from a lead (Sarah's Lake) during the SHEBA field experiment in 1998 (Pegau and Paulson, submitted manuscript, 2002).

problems. As a proxy of what happened beneath the ice during the SHEBA summer time period, we present vertical profiles (Figure 1) taken from a lead (known as Sarah's Lake) (W. S. Pegau and C. A. Paulson, Summertime thermohaline evolution of an Arctic lead, submitted to *Journal of Geophysics Research*, 2002, hereinafter referred to as Pegau and Paulson, submitted manuscript, 2002). During most of July, winds were weak and solar radiation was near the annual maximum. Without significant ice motion, turbulent transport was limited by strong upper ocean stratification produced as low-salinity meltwater accumulated in leads and just beneath the ice. By the middle of July, the depth of modified meltwater was about 1.25 m, as shown by the temperature and salinity profile on 22 July in Figure 1. Ice draft in the vicinity of the lead was about 0.75 m, indicating that ~0.5 m of fresh water was underneath the surrounding ice pack. Helicopter surveys of nearby leads also showed a 0.5-m fresh layer, suggesting that leads were linked by the under-ice fresh layer (Pegau and Paulson, submitted manuscript, 2002).

[5] Bottom ablation rates measured from multiple ice gauges during late July were ~0.5 cm d^{-1} [*Perovich et al.*, 2003] and did not balance the incoming solar flux, indicating that ice melting may have been limited by the strong stratification produced by the fresh layer under the ice. Solar radiation penetrating beneath the ice was effectively trapped below the fresh layer, limiting melting rates [see *Perovich et al.*, 2003, Figure 15]. When winds increased in late July, the fresh layer under the ice was destroyed, as shown by the change in the salinity profiles between 22 July and 28 July 1998. Ice motion during this event caused a rapid mixing of the near-bottom fresh layer and a substantial increase in the average ice bottom melting rate from ~0.5 cm d^{-1} to a maximum of over 1 cm d^{-1} [*Perovich et al.*, 2003]. Estimates of heat flux between the ocean and ice also jumped upward at this time from ~10 to ~30 W m^{-2}, reflecting the increased vertical heat flux and melting rates [*Perovich and Elder*, 2002]. On 28 July, the leads still contained relatively fresh water but this eventually mixed downward, as shown by the profiles on 1 August. Final removal of the fresh layer in the lead was forced by both shear-generated mixing and ice dynamics; the lead size increased dramatically because of ice divergence.

[6] The initial rapid mixing event (between 22 and 28 July) accompanying the increased ice motion was likely a result of two turbulence mixing mechanisms, both related to the ice bottom roughness. The first mechanism relates to the formation of a sheared boundary layer beneath the aerodynamically rough ice. In this case, shear production of turbulence gradually erodes the stable layer as the under-ice fresh layer accelerates along with the ice. Turbulence causes entrainment of the fresh layer into the underlying seawater, leading to a decrease in stratification as more saline water is mixed with the thin fresh layer. A second, more direct effect of ice motion is the destruction of the fresh layer by larger-scale under-ice roughness elements created by ice keels and depressions. Our focus in this paper is on this mixing process, which occurs over very short time periods relative to shear production of turbulence. As the ice begins accelerating, keels with scales greater than ~0.5 m cause large vertical displacements of the fresh layer, much like mountains impinging on flow in the atmosphere. In the under-ice boundary layer, keels can extend vertically 1–10 m and therefore may have a profound influence on the local mixing rates. These effects were noted during SHEBA at one of the turbulence measurement sites located downstream from a ~10-m keel. Turbulence heat fluxes at this sight were measured with values exceeding 100 W m^{-2} or about 20 times routine background flux values.

[7] Although the SHEBA data set provides a wealth of data describing the total heat flux and ice balance during the summer melt period, details of the mixing processes are incomplete and cannot easily tell us how various processes contributed to the vertical flux of heat and salt. In this study, we augment the SHEBA data set by applying a large-eddy simulation (LES) model to the problem of shear- and keel-generated turbulence. This work follows earlier research

reported by *Skyllingstad and Denbo* [2001] that dealt with the role of leads and under-ice mixing during unstable convective conditions. Here we utilize the coupled ice-ocean turbulence model employed by Skyllingstad and Denbo, but with modifications to simulate a series of keels. These modifications are described in section 2 along with the experimental parameters used in the current study.

[8] Our results are presented in section 3 and focus on two different scenarios encountered during the SHEBA field program. In the first case, we examine the role of deep keels during the spring time period when the under-ice boundary layer is relatively deep. Observations of turbulent fluxes downstream from a keel are used to validate the LES model for this case. The second case we examine focuses on the summer fresh layer "mix out" discussed above. Simulations of the fresh layer interaction with different keel depths and ice velocities are presented to determine what factors lead to the destruction of the surface fresh layer. We focus primarily on keel-generated turbulence and the role of fresh water during the summer melt season. Ice edge turbulence is not examined here but will be the topic of a future paper focusing on mixing within a lead. Other ice features that would likely occur under realistic sea ice conditions include depressions and pockets that could isolate water from the main turbulent flow. We do not consider these types of conditions directly in this work. However, because the model uses periodic lateral boundaries we find that small spacing between simulated keels can effectively trap water, much like a refrozen lead or depression in the ice. The consequences of this effect are discussed in the results section of the paper. The paper is concluded in section 4.

2. Model Modifications and Experimental Design

[9] The basis for our experiments is the coupled ice/LES model described by *Skyllingstad and Denbo* [2001]. Ice in this model is represented by a simple slab with an assumed linear temperature profile and imposed surface heat flux [*Maykut*, 1978]. Heat and salt exchange across the ice/ocean interface is governed by transfer coefficients following the work of *McPhee et al.* [1987], which account for the differing molecular diffusivities of heat and salt in seawater. These transfer coefficients apply to both freezing and melting and are therefore not modified in the current application.

[10] Modifications were made to the coupled model so that under-ice roughness elements could directly influence the vertical velocity at the ice/ocean interface through an "orographic" under-ice surface. A discussion of these modifications for bottom boundary roughness elements is presented by *Skyllingstad and Wijesekera* [2003] and repeated here for the upper boundary ice conditions. A number of options exist for simulating variable orography in hydrodynamic models. One method is to perform a coordinate transformation defining a "terrain following" system so that the model grid follows the imposed boundary. This has the advantage of using a concise equation set with smooth flow transitions but must be used with caution when the boundary changes rapidly over short distances. There is also some question regarding the effect of the coordinate transform on turbulent eddies that are assumed to have isotropic properties. A less complicated approach is to simply set the model grid velocity to zero in regions intersected by the ice boundary, creating a stair-step boundary to represent a sloping ice surface (see Figure 2). Besides being easy to implement, this method has the advantage of allowing for sharp keel structures and lead edges, which are common features in open ocean ice packs.

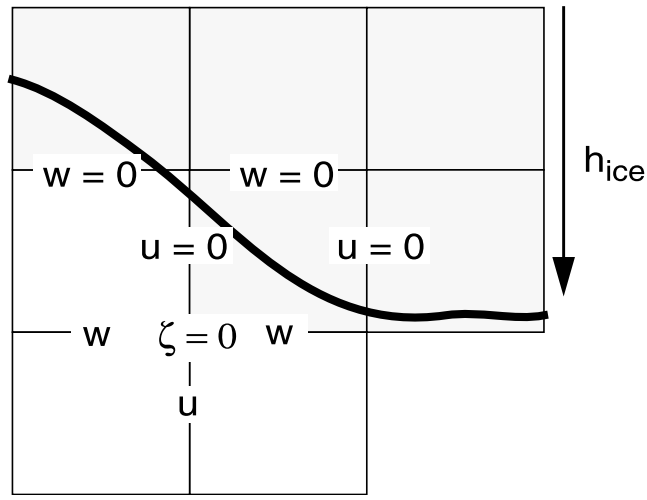

Figure 2. Schematic representation of the ice bottom showing step orography approach. Grid cells having more than 50% ice are considered solid ice, and velocities are set to zero.

[11] The main disadvantage of the step topography scheme is the generation of noise at the corner points and possible increase in the effective roughness because of enhanced subgrid-scale mixing. To overcome this problem, *Gallus and Klemp* [2000] used a boundary condition on their momentum transport equation that effectively set the vorticity, ζ, at topographic corner points to zero (see Figure 2). A similar method is applied here, but in place of the advective form for the equations of motion, we use an enstrophy-conserving scheme following *Tripoli* [1992],

$$\frac{\partial u_i}{\partial t} = \varepsilon_{ijk} u_i \eta_k - \frac{\partial}{\partial x_i}\mathrm{KE} - \frac{\partial}{\partial x_j}\langle u_i'' u_j'' \rangle - \frac{\partial \tilde{P}}{\partial x_i} - \delta_{i3} g \frac{\rho'}{\rho_0} + \gamma \partial^{12} u_i, \tag{1}$$

where

$$\langle u_i'' u_j'' \rangle = -K_m \left(\frac{\partial u_i}{\partial x_j} + \frac{\partial u_j}{\partial x_i} \right), \; \tilde{P} = \frac{P}{\rho_0} + \frac{2}{3}\bar{q}^2,$$

$$\eta_k = \zeta_k + f_k, \; \zeta_k = \varepsilon_{kij} \left(\frac{\partial u_j}{\partial x_i} \right), \; \mathrm{KE} = \frac{1}{2} u_i^2,$$

u_i are the Cartesian velocity components, t is time, g is the acceleration of gravity, δ_{i3} is the Kronecker delta, $\varepsilon_{i,j,k}$ is the antisymmetric tensor, P is pressure, ρ' is the perturbation density, ρ_0 is a constant average density, K_m is the subgrid-scale eddy viscosity, $\bar{q}^2$ is the subgrid-scale turbulent kinetic energy, f_k are components of the Coriolis term, and $\gamma \partial^{12} u_i$ is a twelfth-order filter with filter coefficient $\gamma = 0.07$ to remove a $2\Delta x$ artifact of the differencing scheme [see *Denbo and Skyllingstad*, 1996]. Double primes denote subgrid-scale fluxes which are parameterized.

[12] Horizontal components of the vorticity, $\zeta_{1,2}$, are calculated on an Arakawa C grid, as shown in Figure 2.

To ensure that the boundary does not generate spurious vorticity, we set the boundary condition $\zeta = 0.0$ for corner points and at the flat ice/water interface. As a test of this scheme, we performed a series of simulations using terrain and flow conditions with scales equivalent to experiments reported by *Long* [1955]. Results from these tests are reported by *Skyllingstad and Wijesekera* [2003] for a version of the model with partial volume grids at the boundary and show good qualitative agreement between the model, analytical, and laboratory results. Here we did not use partial volumes at the ice water boundary but simulated changes in ice thickness using full grid cell blocks. This introduces small-scale motions but is not unrealistic, given the uneven nature of the ice bottom surface.

[13] Momentum flux between the ice and ocean in the model is simulated using a bulk drag relationship

$$\langle u_i'' u_3'' \rangle = C_D \Delta u_i |\Delta u_i| = u_*^2, \tag{2}$$

where

$$C_D = \left[\frac{\kappa}{\ln(\delta z / z_0)} \right]^2, \quad \Delta u_i = U_{\text{ice}} - u_i(z_1),$$

$\delta z = 1/2\Delta z$, Δz is the grid spacing, z_1 is the first grid level below the ice, $\kappa = 0.4$ is the Von Karman constant, and z_0 is the roughness length and is set to 0.005 m following *McPhee* [2002]. Surface momentum flux is also referenced through a "friction velocity" or u_*, as indicated in equation (2). For a complete description of the ice/ocean model, the reader is referred to the work of *Skyllingstad and Denbo* [2001].

[14] Ice bottom orography was set using a "witch of Agnesi" profile modified by an along-ridge sinusoidal variation,

$$h = \frac{h_{\max} a^2}{x^2 + a^2} \left(1 + \sin 4\pi \frac{y}{y_{\max}} \right),$$

where $h_{\max}$ is the maximum height, a is the half-width of the obstacle, and $y_{\max}$ is the y axis width, and x is displaced to the center of the domain. Actual ice keels are usually complex structures with multiple sharp edges and variations that are created when the ice pack is tilted vertically during compression. As a first approximation to this variability, we applied along-axis variation to encourage the development of three-dimensional turbulence eddies.

[15] Simulations were initialized at rest with a linearly increasing, imposed ice velocity. The model was operated using a reference frame moving with the ice velocity, i.e., a mean velocity was imposed equal to the ice velocity. Results, however, are shown using a reference frame at a fixed geographical location, as though the ice were moving from right to left.

[16] We could not realistically increase the ice velocity as would occur in actual wind events because of the long timescale of storms and the very small time step required by the LES model. As a consequence, our results do not represent the effects of orography on fully developed turbulent flows but are more representative of the turbulent processes directly attributable to ice bottom features. Lateral boundaries in the model were set to periodic conditions, which effectively means that our simulations represent flow over a series of ice keels or ridges rather than a single bottom obstruction. For stratified flow conditions, the periodic boundaries can cause the near ice flow to gradually stagnate as water is trapped by the keel. Early in the simulations, the action of the keel on the flow is much like an isolated feature, but as time progresses, the flow behaves more like flow over a depression in the ice with trapped water. The time needed for flow stagnation varies with the initial conditions, therefore specific ice velocities and spin-up periods are given in the introductions to each of the experiments.

3. Results

[17] We considered two scenarios for examining the effects of keels on upper ocean turbulence. The first scenario was designed to simulate conditions observed during March 1998 from a turbulence mast deployed at the SHEBA site downstream from a pressure ridge. Observations of turbulent flux quantities from the mast showed periods of intense mixing, most likely in response to flow disruption as water moved under the keel. These observations were unique in that typical turbulence levels measured away from keels were much weaker.

[18] Our second scenario focuses on summer time conditions when stratification is very strong because of ice melt and fresh water accumulation in leads and beneath the ice. We are interested in understanding how keels affect mixing of the under-ice fresh surface when wind forcing moves the ice. During SHEBA, the fresh layer was destroyed in a matter of days when ice motion increased dramatically in late July/early August. Unfortunately, turbulence measurements are not available for this time period, and we are limited to only conductivity-temperature-depth (CTD) data collected from leads. Nevertheless, results from the LES model can help in understanding what role keels might have had in the fresh layer mixout process.

3.1. Case 1: Spring Well-Mixed Boundary Layer, SHEBA, March 1998

3.1.1. Field Data

[19] A primary task of the SHEBA field experiment was the collection of oceanic heat flux measurements, which include turbulence profiles in the upper ocean beneath sea ice under a wide range of conditions. Sensors capable of high-frequency measurements of temperature, salinity, and velocity measurements were deployed on a vertical mast at depths ranging from $\sim$1 m beneath the ice to a depth of $\sim$12 m. Most of the time, turbulent fluxes behaved in a manner consistent with a wall layer, suggesting that the ice bottom can be characterized as an aerodynamic rough surface. *McPhee* [2002] used this observation to estimate an average value for the roughness length under ice, $z_0 = 0.005$ m, which for the most part describes the ice bottom characteristics. However, exceptions to this rule did occur when the instrumented mast was located near leads and keels (the mast was moved a number of times either to avoid damage from ice motion or to measure flow under different ice characteristics). Measurements in these

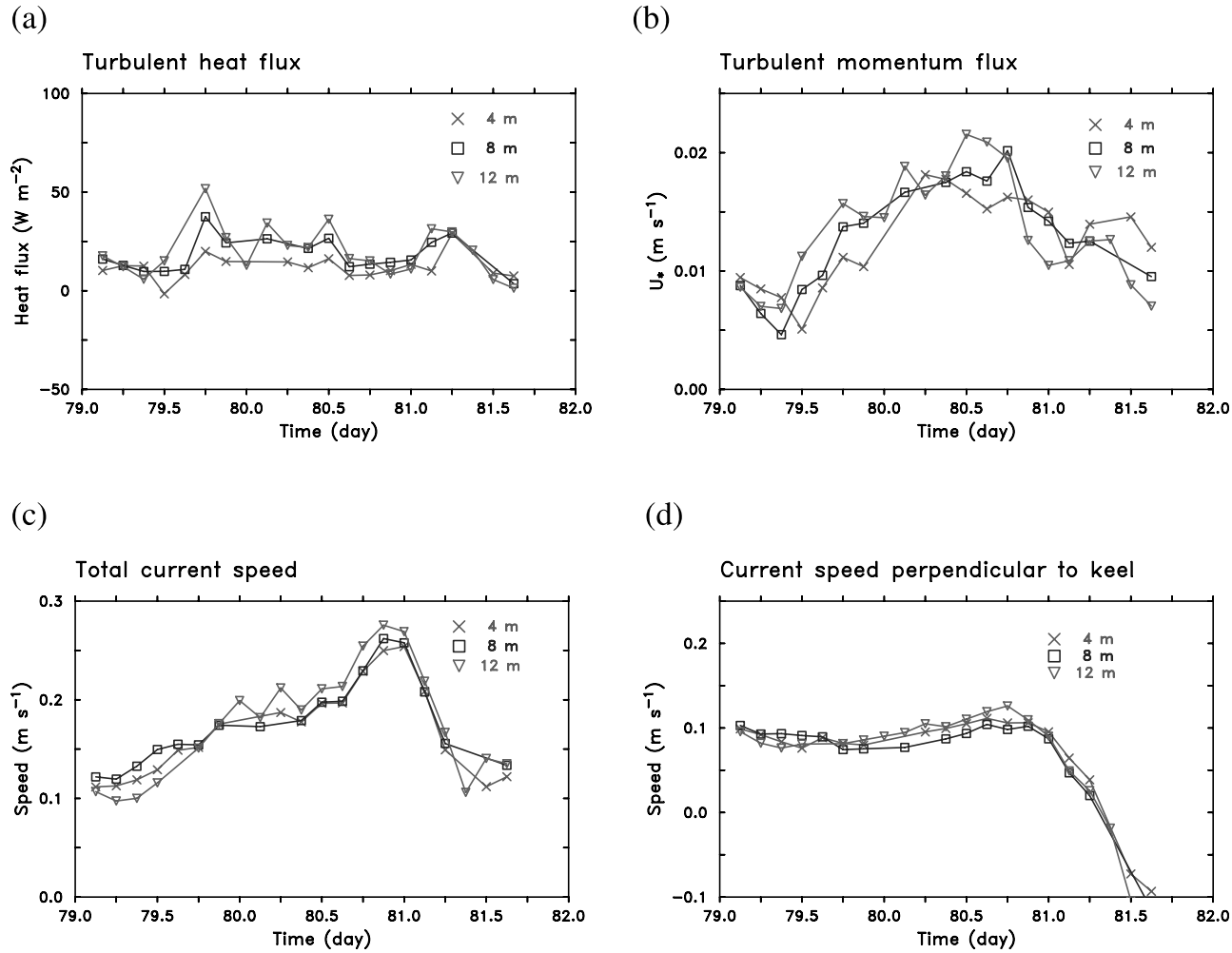

Figure 3. (a) Turbulent heat flux, (b) friction velocity, (c) total current speed, and (d) current speed perpendicular to the keel averaged over 3-hour periods from days 79 to 82 during the SHEBA field experiment. Fluxes are calculated from turbulence velocity data and fast response thermistors deployed on a rigid mast below the ice.

locations produced some of the most significant turbulent fluxes during the field experiment.

[20] One time period in particular, days 79–82 (19–22 March) 1998 shown in Figure 3, demonstrates how the under-ice boundary layer was affected by flow passing under a ~10-m-deep ice keel. Turbulent flux data shown in Figure 3 were calculated using 3-hour averages of friction velocity, u_*, and turbulent heat flux,

$$u_* = \sqrt{u'w'}, \quad w'T', \tag{3}$$

where primes denote perturbations from 15-min averages. The location of the mast containing the turbulence instruments was roughly 100 m downstream from the keel. Data collection did not begin until day 78 because of technical problems associated with the ice motion. Even so, initial heat flux values of up to 400 W m^{-2} were observed on day 78 (not shown) before settling down to near-steady values of ~25 W m^{-2} on days 79–80. At the same time, flux measurements made away from the keel using an acoustic travel-time-based instrument (not shown) indicate much lower flux values between 2 and 10 W m^{-2}, more in line with smooth ice boundary layer values. Average currents during the 2-day period increased from ~0.1 m s^{-1} to a maximum value of ~0.25 m s^{-1} on day 81 before falling off to ~0.1 m s^{-1} at the end of the record (Figure 3c). The current direction also changed from an angle roughly perpendicular to the ice keel to a direction more parallel with the keel orientation over this time period, eventually reversing direction so that the mast was upstream from the keel at the end of the time series. Using estimates of the keel orientation, a transformed velocity time series was produced with components parallel and perpendicular to the keel. As shown by the perpendicular component (Figure 3d), the reduction in turbulent fluxes at the site of the mast after day 81 (Figure 3b) could be attributed to the reduction and reversal in the cross-keel flow. The very large turbulent flux values (~400 W m^{-2}) measured on day 78 (not shown here) do not appear to be a function of the current velocity, indicating that transient effects may have produced the initial elevated flux values. Because the fluxes are more consistent with the flow velocity data after day 78, we focus our initial modeling experiments on this time period.

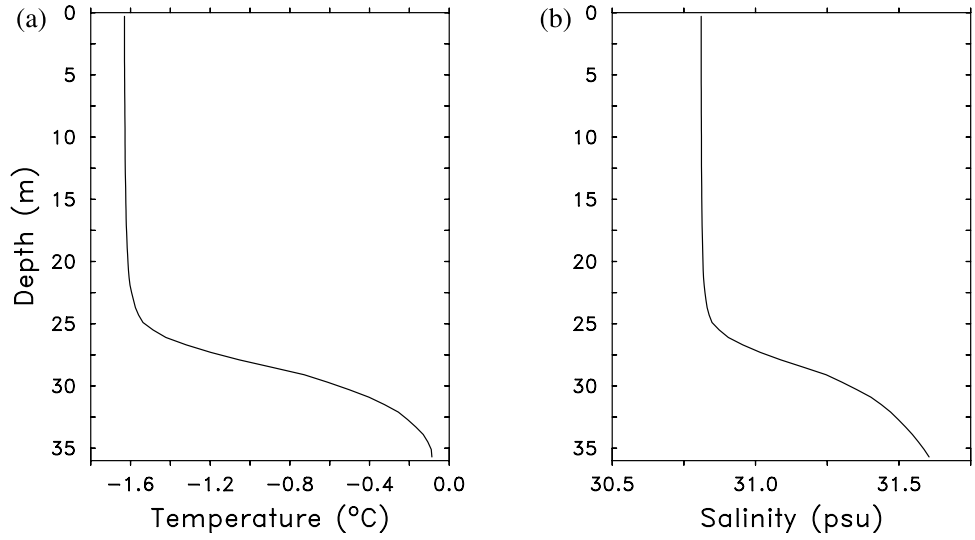

Figure 4. Initial profiles of (a) temperature and (b) salinity taken from conductivity-temperature-depth (CTD) cast made on day 79.

3.1.2. Simulated Structure

[21] Simulations for this case were performed using an initial profile of temperature and salinity taken from a CTD cast made on day 79 (19 March 1998) (Figure 4). The mixed layer at this time was ~25 m deep with a surface temperature slightly above freezing (−1.63° versus −1.68°C). Ice motion was set to 0.1 m s^{-1} in the cross-keel direction and 0.17 m s^{-1} in the along-keel direction, which yields a speed of 0.2 m s^{-1}, similar to the speed between days 79 and 80 shown in Figure 3c. Spatial dimensions for the simulation were 614.4 m in the x or cross-keel direction, 76.8 m in the y or along-keel direction, and 36 m in the vertical direction, with a resolution of 0.6 m (grid dimensions of 1024 × 128 × 60). A channel domain was selected so that the cross-obstacle flow would have a greater distance of travel before recirculating through the domain. Simulations were performed on a 32-processor IBM SP-3. Parallelization of the model utilized the Message Passing Interface (MPI), with the domain divided along the x axis, i.e., each subdomain was of grid size 32 × 128 × 60. Two keel heights were considered: 10.8 m or 18 grid points for the deep-keel case representing the mast data presented above and 1.8 m or 3 grid points representing conditions away from the keel under the ice pack. The length of the simulations was 2 hours for the deep-keel case and 3 hours for the shallow-keel case. The deep-keel case was of limited duration to prevent significant alteration in the upstream boundary layer structure resulting from using periodic boundaries. A longer run time was possible in the shallow-keel case because of the weaker turbulence response to the keel.

[22] Vertical-cross-section plots of the simulated u velocity component (cross keel) and salinity (Figure 5) for each keel depth demonstrate how the deep keel affects the turbulent boundary layer in comparison with the shallow keel (keel motion is from right to left). For the deep-keel case, the velocity field is characterized by a gradual increase in the horizontal velocity over the keel, followed by a turbulent wake or separation zone in the lee of the keel. In the wake region, the water is moving very near the velocity of the ice, indicating that a recirculation zone is active within ~25 m of the keel. Further downstream, velocities are more turbulent, with flow gradually decreasing in speed from the ice velocity of −0.1 m s^{-1} to about −0.05 m s^{-1} at the edge of the plot. Turbulence in the wake region extends from the ice bottom to the halocline at ~25-m depth. Perturbations in the halocline are noted downstream from x = ~350 m and represent regions of active entrainment of more saline water into the boundary layer.

[23] In contrast to the deep-keel case, the shallow-keel simulation displays a more uniform boundary layer structure. The influence of the keel on the boundary layer is much less significant in comparison with the deep-keel case, with almost no variation in turbulence downstream from the keel. Perturbations in the halocline do not appear in this case, indicating that the short keel does not promote significant growth of the boundary layer or vertical transport of warmer, saltier water up to the ice bottom (which promotes faster melting).

3.1.3. Simulated Fluxes

[24] Simulated values of the cross-stream-averaged turbulent heat flux are shown in Figure 6, corresponding to the time of the cross sections shown in Figure 5. Vertical motions generated by the keel actively generate regions of upward and downward heat flux that extend through the boundary layer. In total, the eddies produce a net upward transport of warmer water from the pycnocline, as shown by the gradual shoaling of the $\theta = -1.6300$°C isotherm. Vertical profiles of horizontally averaged heat flux (Figure 7) quantify the overall effects of the keel by showing a large increase in the upward flux of momentum and heat when the keel depth is increased from 1.8 to 10.8 m. Comparison of the simulated heat flux to measurements shown in Figure 3 on day 80 (corresponding to a total current speed of 0.2 m s^{-1} as in the simulation) indicates overall good agreement in the magnitude and vertical distribution of the turbulent heat flux. The measurements indicate an increase in heat flux from about 10–15 W m^{-2} at 4-m depth to ~25 W m^{-2} at 12 m, whereas

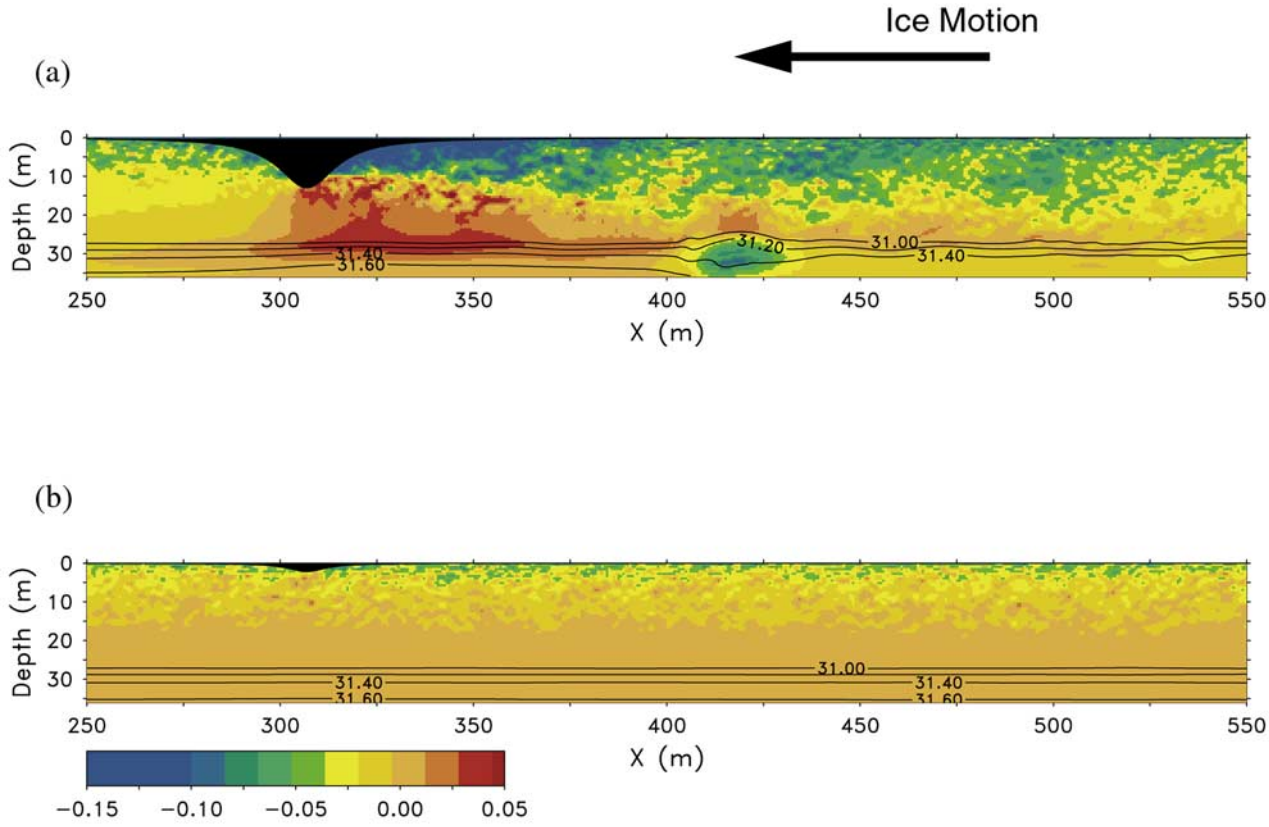

Figure 5. Vertical cross section of the u velocity component (shaded, m s^{-1}) and salinity (contours, practical salinity unit (psu)) for a keel height of (a) 10.8 m taken at hour 2 and (b) 1.8 m taken at hour 3. Both plots are from y = 18.9 m. Also shown is the keel profile centered at x = 307.2. Ice motion is from right to left.

the model values increase from ~10 to ~30 W m^{-2}. The range of modeled turbulent heat flux values are also similar to the monthly average ocean heat flux estimate of 15 W m^{-2} made by *Perovich and Elder* [2002] based on measurements of ice heat conductance and ice mass balance, suggesting that keels were important in determining the heat balance. As shown in Figure 7, upward heat transport into the boundary layer is as high as 100 W m^{-2} near the keel. Consequently, even a small number of keels could boost average upward heat flux into the boundary layer and affect ice bottom freezing/melting rates.

[25] Comparison of the simulated momentum flux also shows good agreement with observed turbulence data at 12-m depth, where the observations show u_* between 0.015 and 0.02 m s^{-1} versus the model value of ~0.012 m s^{-1}. Closer to the ice bottom, however, the simulated u_* of

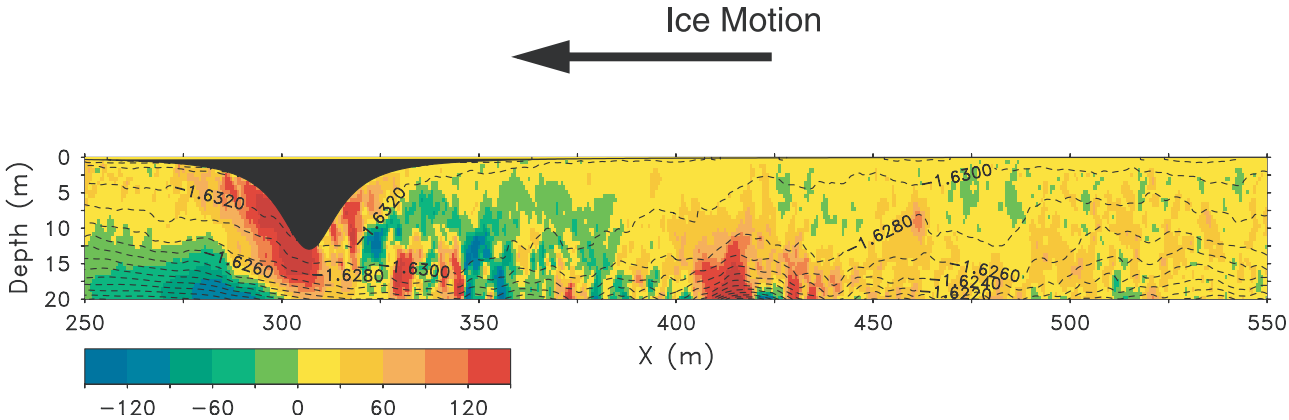

Figure 6. Cross-stream-averaged turbulence heat flux, $\overline{w'\theta'}$, (W m^{-2}) and potential temperature, θ, (°C) from hour 2 of the 10.8- m keel case showing plumes of warmer water that are forced upward by turbulence at the pycnocline interface between z = 15 and 20 m.

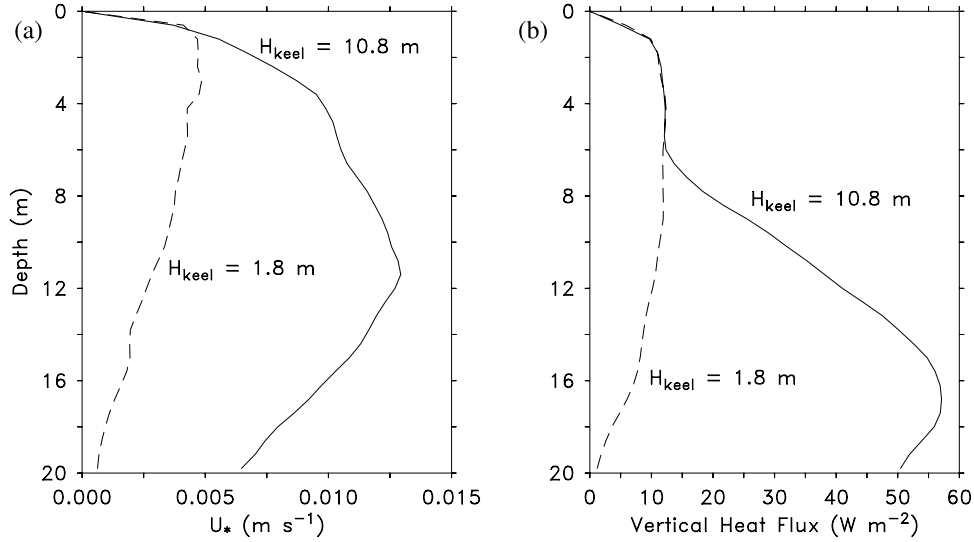

Figure 7. Horizontal averages of the (a) turbulent heat flux, $\overline{w'\theta'}$, and (b) friction velocity, $u_* = \sqrt{\overline{u'w'}}$, calculated at t = 2 hours for keel depth of 10.8 m and t = 3 hours for keel depth of 1.8 m.

0.01 m s^{-1} is about two thirds the observed value of ~0.015 m s^{-1} at 4 m. Discrepancies between the simulated and measured momentum flux could be a result of the simulation having a relatively smooth ice bottom surface away from the keel. The actual ice bottom surface would likely have O (1 m) ice deformations on and around the keel, which would generate larger values of u_* without greatly affecting the upward heat flux that is linked to mixed-layer entrainment.

3.1.4. Ice Bottom Fluxes

[26] Polar winter conditions are typically cold enough so that ice is constantly forming at the bottom of the ice pack. Flow over keels, however, can reverse this process if enough heat is transported by turbulence from below the mixed layer to balance the flux through the ice. During the time period presented in Figure 3, the SHEBA station was located over a region of water with a freezing point about 0.03°C below the observed temperature. Consequently, sea ice was only forming if the heat loss through the ice could overcome the transfer of heat from the seawater. Ice thickness measurements taken in March confirmed that ice was melting, even though surface air temperatures were at times −30°C [*Perovich et al.*, 2003; *Perovich and Elder*, 2002]. Our assumptions of 2-m-thick ice and 0.5 m of snow provided enough insulation so that simulated ice was always melting. Typical upward heat fluxes in the model ice were ~7 W m^{-2}, versus the ~12 W m^{-2} ocean turbulent fluxes noted above, and ice bottom melting fluxes were ~16 W m^{-2}. As a result, ice melting was effectively cooling the seawater just beneath the simulated ice at a rate of about 11 W m^{-2}. While the simulated keel turbulence did not determine if the ice was melting or freezing, plots of the ice bottom flux from the model averaged across the flow (Figure 8) show that the keel does affect the local ice melting rate by increasing the turbulent heat transport near the ice bottom. Fluxes in the vicinity of the ice keel actually show a strong decrease in the relatively quiescent wake region immediately downstream from the keel where the water is moving at nearly the same speed as the ice. Elsewhere, however, the melting heat flux is about 2 W m^{-2} larger in the 10.8-m keel case in comparison with the 1.8-m keel case.

3.2. Case 2: Summer Fresh Layer, SHEBA, July 1998

3.2.1. Simulation

[27] In the introduction, we presented profiles of temperature and salinity from the summer melt period (Figure 1), showing how melting ice generated a strongly stratified layer about 0.5 m beneath the ice. Ice motion at the end of July forced a rapid mixing of this fresh layer with the underlying boundary layer over a period of a few days. Turbulence data were not collected during this time period, so we rely on the LES model to provide insight on the processes that might have caused the rapid mixing of the fresh layer. In particular, we investigate the role of small keels on the initial mixing of the fresh layer.

[28] The stratified fresh layer structure can be viewed as a two-fluid system, with the top layer having lower density in comparison with the underlying ocean. Interaction of the

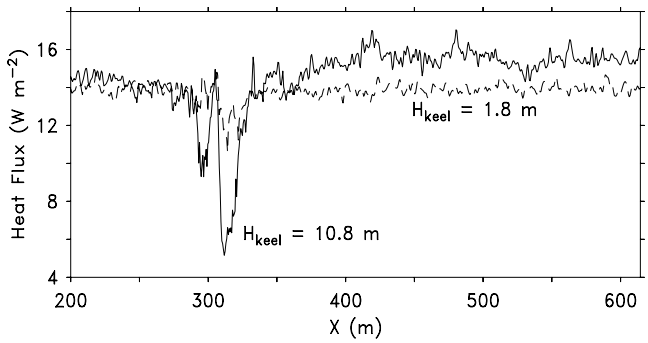

Figure 8. Ice bottom heat flux averaged in the cross-stream direction for the March simulations with keel depths of 10.8 m (solid) and 1.8 m (dashed). Heat flux in the simulations is upward, indicating melting of the ice and cooling of the ocean.

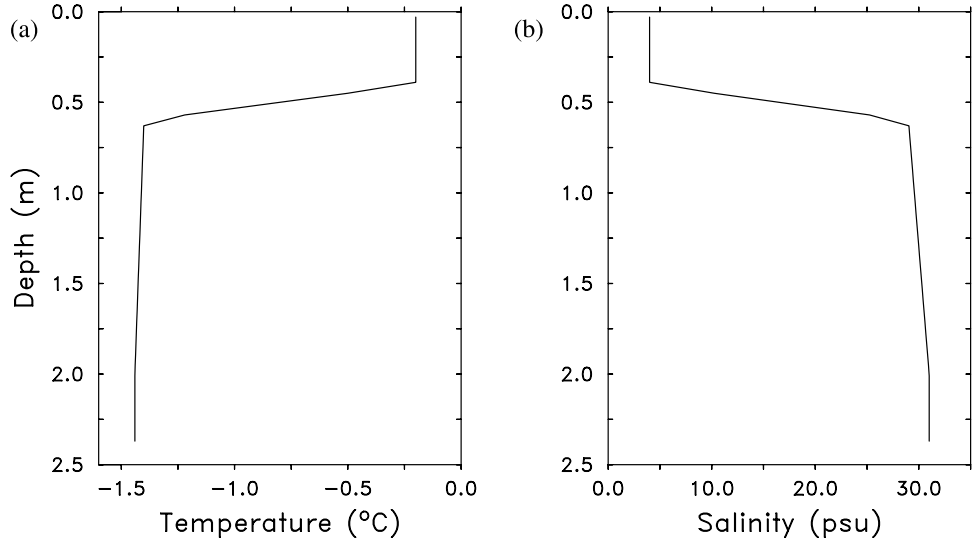

Figure 9. Initial conditions of (a) potential temperature (°C) and (b) salinity (psu) representing under-ice conditions during late July 1998. The ice bottom begins at a depth of 0 m.

fresh layer with keels is governed by hydraulic flow principles that depend on the value of a Froude number defined as

$$F = \frac{U}{\sqrt{(g\prime h_1)}}, \quad g\prime = g\frac{(\rho_2 - \rho_1)}{\rho_1}, \tag{4}$$

where g is gravity, h_1 is the depth of the fresh layer, ρ_1 and ρ_2 represent the density of the fresh layer and ambient ocean, respectively, and U is the speed of the ice. For shallow keels, the flow can be subcritical ($F < 1$), supercritical ($F > 1$), or transcritical, where F changes from subcritical to supercritical when passing over the keel. Transcritical flows are typically more energetic and can force turbulent mixing downstream of the keel when the flow transitions back to subcritical flow through a hydraulic jump.

[29] If the keel depth is a significant fraction of the fresh layer depth and $F < 1$ upstream from the keel, then a slightly different flow scenario can develop. In this case, the flow is blocked upstream from the keel, which changes the effective depth of the flow going over the keel and can generate a transcritical flow scenario. Downstream from the keel the flow is again subcritical, causing the formation of a stationary hydraulic jump followed by lee waves [e.g., *Baines*, 1995, see pp. 104 and 132]. Because the fresh layer under undeformed ice was only ~0.5 m deeper than the summer time first-year ice draft, we suspect that blocking was a common occurrence during the SHEBA mixing-out period in late July. Simulations presented here examine a range of keel depths to determine how the fresh layer responds when forced over keels.

[30] Initial condition profiles of temperature and salinity for the summer fresh layer case are shown in Figure 9. These profiles were taken from the measurements shown in Figure 1 by assuming an ice thickness of ~1 m and then reducing the temperature to the freezing point in the upper portion of the fresh layer that would be adjacent to the pack ice. Our intent was to produce a profile that best represents the fresh layer beneath the ice some distance from an open lead. Although the fresh layer is similar to the idealized flow scenario described by equation (4), in reality the profile is stratified so that a single value for ρ_1 cannot be given. Nevertheless, a range of F can be made by using the average density of the fresh layer (ρ = ~1003 kg m^{-3}) and the ambient seawater (ρ = ~1024 kg m^{-3}) with a fresh layer depth of h_1 = 0.5 m. Using these values yields a transition from subcritical to supercritical flow when U rises above ~0.32 m s^{-1}. Typical values of ice velocity during SHEBA were about 0.06 m s^{-1} before the late July wind event, increasing to ~0.43 m s^{-1} when the winds increased [*Perovich and Elder*, 2002]. Consequently, as ice accelerated in late July, flow conditions probably encompassed blocking subcritical, transition, and supercritical flows.

[31] Three experiments were performed using the initial conditions shown in Figure 9. The model grid in each experiment was set to 1600 points in the x direction, 128 points in the y direction, and 40 vertical levels. In the first two experiments, which will be referred to as the "small keel" cases, we focused on small under-ice variations by setting the keel depth to 0.18 and 0.54 m, with a grid resolution of 0.06 m. Larger keels were considered in the third experiment by setting the keel depth to 1.0 m, with the grid spacing increased to 0.2 m. This experiment will be referred to as the "large keel" case. Ice velocity in the small keel simulations was initially set to 0.0 m s^{-1} and then linearly increased to 0.25 m s^{-1} over the first 10 min of the simulation. The 0.25 m s^{-1} ice velocity was selected as representing transition flow conditions that could have occurred at the onset of the wind event. Total run length in these cases was 20 min. In the third simulation, ice velocity was linearly increased from 0 to 0.43 m s^{-1} over the initial 60 min. We chose the higher ice speed in this case to represent the average ice motion (0.43 m s^{-1}) that occurred on 29 July [*Perovich and Elder*, 2002]. The large keel simulation was ended after 1.5 hours.

[32] In all the simulations, the relatively rapid increase in the ice speed is much larger than would likely be encountered in the Arctic (except perhaps in coastal regions with tides).

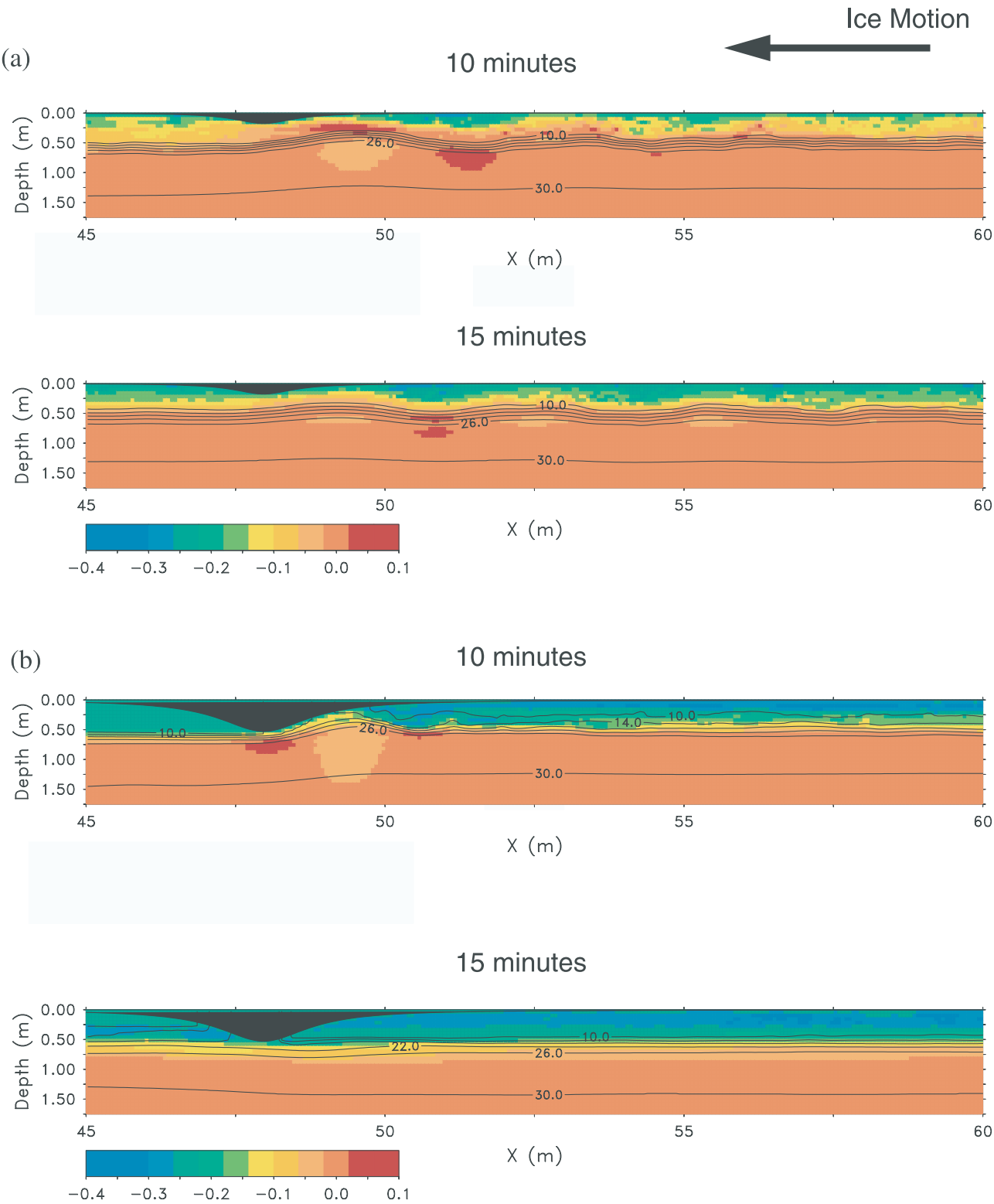

Figure 10. Vertical cross section from $y = 1.9$ m of the u velocity component (shaded m s^{-1}) and salinity (contours, psu) for a keel height of (a) 0.18 m after 10 and 15 min and (b) 0.54 m after 10 and 15 min.

Nevertheless, we find that after a brief adjustment phase, the cross-keel flow appears to develop an equilibrium behavior similar to hydraulic transition flows. Over time the flow gradually changes as the mean state is affected by mixing. We think that the hydraulic control phase of the flow is representative of flow behavior over a relatively isolated keel. However, because the ice velocity is initialized in a fairly unrealistic way, our results should be viewed with caution.

[33] Results from the small keel cases are presented in Figure 10, showing cross-section plots of the velocity and

salinity after 10 and 15 min for the two keel depths. At 10 min, flow behavior in both cases shows similarities to transition flows, as described above. For the 0.18-m keel case, the keel is completely within the fresh layer but constricts the flow enough so that a transition from subcritical to supercritical flow occurs at the crest of the keel. In response, the flow accelerates in the lee of the keel and generates a train of weak internal lee waves similar to laboratory experiments presented by *Baines and Hoinka* [1985], although here the flow is not uniformly stratified. Over time, blocking of the flow is evident ahead of the keel and the average velocity gradually approaches the ice speed as the fresh layer picks up momentum from the keel pressure drag and surface friction. Mixing of the fresh layer in this case is a relatively slow process because the lee wave disturbances do not overturn or increase the local shear to critical levels.

[34] In the 0.54-m keel case, most of the fresh layer is blocked by the obstacle so that only a thin layer of less salty water is forced over the keel. This layer accelerates on the lee side of the keel and rapidly readjusts in a region of chaotic flow downstream from the keel, in a manner similar to a transitional hydraulic flow with a downstream jump. Perturbations in the flow downstream from the jump actively mix the stratified layer, as shown by visually comparing the vertical gradient of salinity in the lee of the keel with the upstream conditions. After 15 min, the effects of blocking of the flow by the keel dominate the simulation, resulting in a slab of low-salinity water that is moving at roughly the ice velocity, bounded just below the depth of the keel by the readjusted stable salinity gradient. At this point the keel has little influence on vertical mixing because it is completely within the relatively uniform fresh layer that is moving at roughly the same speed as the ice.

[35] A large portion of the momentum transfer between ice and ocean occurs through pressure drag exerted by the ice keel on the ocean. We can calculate this drag by spatially averaging the horizontal pressure term in the momentum equation in the x and y directions,

$$P_{\text{drag}} = \sum_{x,y} \frac{1}{\rho} \frac{\partial P}{\partial x}, \tag{5}$$

where P is the pressure and ρ is the density. The second source of momentum transfer is the aerodynamic drag produced by ice bottom friction. We calculate the aerodynamic drag by subtracting the pressure drag term from the total velocity change, $\frac{\partial u}{\partial t}$. The reason for computing aerodynamic drag this way, rather than from equation (2), is to account for ice bottom friction produced by the discrete grid representation of the ice keel.

[36] Plots of P_{drag} for the two keel depths and the residual aerodynamic drag (Figure 11) demonstrate how the 0.54-m keel produces a stronger pressure deceleration in the flow relative to the 0.18-m keel. In contrast, the ice bottom aerodynamic drag in the 0.18-m case is stronger because the ice velocity relative to the ocean is greater at the end of the 10-min spin-up period. The 0.54-m keel pressure drag peaks at about 6 min and then decreases as the water above the keel depth slows down to match the ice velocity. After $\sim$13 min, the pressure drag reverses direction for a brief period of time, possibly because of readjustment or sloshing

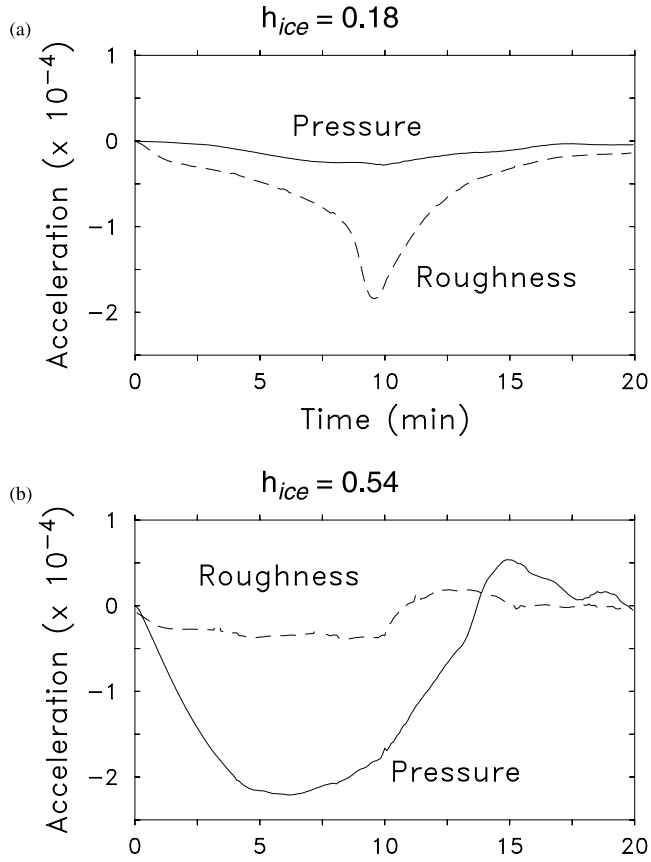

Figure 11. Vertically and horizontally averaged horizontal momentum terms accounting for changes in momentum due to pressure and ice bottom roughness for keel depths of (a) 0.18 m and (b) 0.54 m. Units are m s^{-2}.

of the fresh layer trapped by the keel. Sloshing is an effect of the period boundaries, which creates a domain configuration similar to a series of keels. Blocking of the flow by the keel stores momentum that is released through a reversed pressure gradient when the transition flow ceases between 10 and 15 min. If flow over keels can be described using a hydraulic approach, then it might be possible to parameterize keel drag and mixing based on the keel-relative Froude number, as given in equation (4). In our simulations, the flow appears to produce a hydraulic response, but the periodic boundary conditions limit the duration of this response.

3.2.2. Ice Melt Heat Flux

[37] The effects of increased vertical mixing produced by the keel simulations is shown by plots of the heat flux used to melt ice at the ice bottom (Figure 12). Ice melting is affected by both the downstream dynamical effects noted above and by the along-keel depth variations. For the 0.18-m keel, the highest heat flux or melting rates occur in regions where the ice relative flow speed is the highest, for example, along the lee-side edge of the keel and between the pockets of slow moving water in the lee wave system. Ice melting is strongly dependent on the friction velocity or u_* (see equation 1) at the ice bottom and on the difference between the water temperature and freezing point, or freezing point depression. Variations in the melting rate

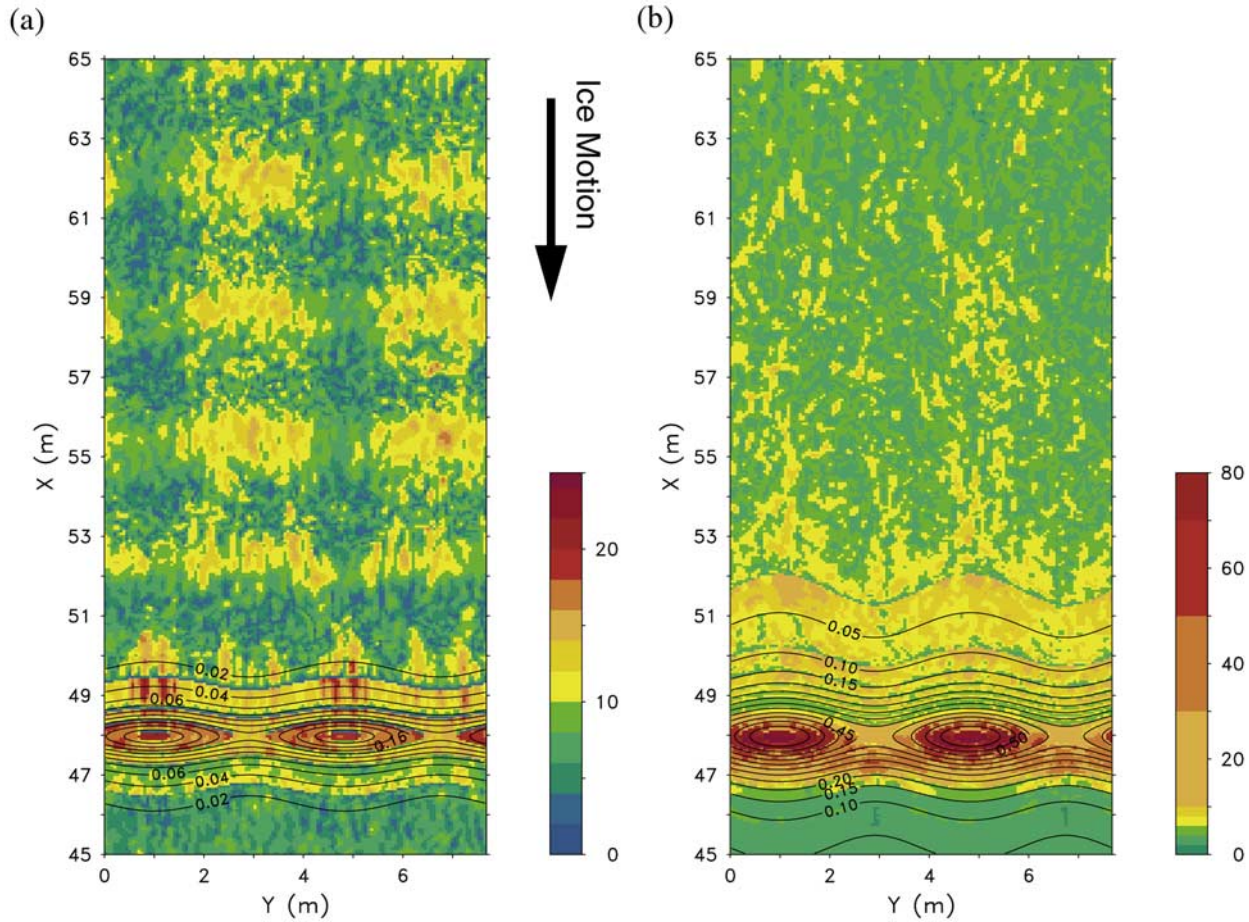

Figure 12. Heat flux (W m^{-2}) used in melting ice for a keel depth of (a) 0.18 m and (b) 0.54 m. Also shown are contours (m) of keel depth. Note the difference in shading levels used in each case.

shown in Figure 12 for the 0.18-m keel are mostly due to increased u_* forced by the difference between the water velocity and the ice speed. Increasing the keel depth to 0.54 m produces much stronger ice melting along the keel ridge and downstream from the keel where water accelerates over the keel barrier. On the keel ridge, both u_* from the ice/water velocity difference and the freezing point depression (the keel extends beneath the fresh layer) act to increase the melting rate and produce fluxes of over 80 W m^{-2}. Fluxes of ~30 W m^{-2} are indicated within the higher-velocity downslope region of the flow in response to the higher u_* in this region.

[38] Our results showing that deeper keels exhibit much higher melting rates is consistent with observations by *Wadhams* [1992] and *Rigby and Hanson* [1976] indicating a dependence of ice melting on ice draft. *Schramm et al.* [2000] examined if the two-dimensional geometry of keels could account for enhanced melting, independent of hydrodynamic effects. They found that ablation rates did increase but were not high enough to explain the observed melting rates of *Wadhams* [1992]. Increased melting rates from flow acceleration, as modeled here, were suggested as a key ablation process. More recent observations from SHEBA reported by *Perovich et al.* [2003] strongly suggest that keels generate higher ablation rates, with deformed ice having average bottom melt 50% larger than undeformed ice. Likewise, estimates of annual average heat flux from the ocean to ice during SHEBA [*Perovich and Elder*, 2002] were highest, 12.1 W m^{-2}, in the region of an old ridge, versus multiyear ice site values of ~7.5 W m^{-2}.

[39] Maximum melt fluxes appear greater in the 0.54-m case when compared to the 0.18-m simulation. However, fluxes in the lee of the 0.54-m keel drop off rapidly to values below 10 W m^{-2} within a distance of ~10 m. In fact, time series plots of the horizontally averaged ice heat flux (Figure 13) show that the total ice melting heat flux is greater throughout the simulation in the 0.18-m keel case in comparison with the 0.54-m case. As noted above, fresh water is trapped by the 0.54-m keel and accelerates to match the ice velocity through pressure drag rather than through turbulent momentum exchange. In contrast, the 0.18-m keel does not cause a strong pressure acceleration, which allows for a greater difference in velocity between the ice and adjacent seawater. Accordingly, u_* (and melting) is greater over a larger area in the 0.18-m keel case when compared with the 0.54-m simulation. These results present a dilemma in trying to parameterize the effects of keels on ice melting rates. As noted above, observations and our model results

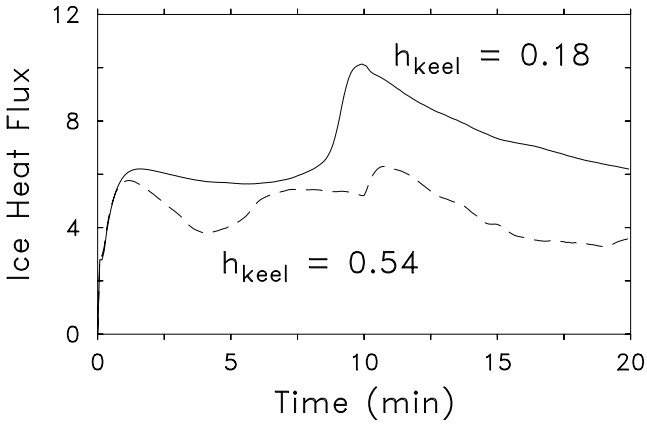

Figure 13. Horizontally averaged ice bottom heat flux (W m^{-2}) as a function of time from July cases with keel depth of 0.18 an 0.54 m. Ice heat flux represents heat that is used to melt ice; heat flux through the ice slab is assumed to be negligible.

yield much higher ablation rates near keels, but our domain average results indicate that large keels can trap water and actually reduce melting over large areas. Because the model uses periodic boundary conditions and is highly idealized, it is likely that natural variability in keel size and shape would prevent as much trapping as is simulated in the model. Therefore melting rates would not decrease away from the keel but would be more representative of a sheared boundary layer. Nevertheless, our results do point out the importance of fresh water trapping in depressions and channels. Water in these areas will insulate the ice bottom from the relatively warmer boundary layer water, slowing down the melting process until shear-generated turbulence can erode away the fresh layer.

3.2.3. Large Keel Simulation

[40] Observed ice acceleration rates in the Arctic are usually much slower than those applied here, with ice taking many hours to reach velocities of 0.25 m s^{-1}. Therefore our small keel results are really only useful in trying to understand possible processes that control ice bottom turbulence. In actual ocean situations, blocking of the flow by keels is dependent on the keel orientation (e.g., as in case 1) and frequency of keel occurrence. Relatively remote keels could generate turbulent mixing similar to the 0.54-m keel model result if upstream conditions are undisturbed. Unfortunately, investigating isolated topographic features with LES is difficult because of the need to define upstream boundary conditions that might contain a turbulent boundary layer. As an alternative, we apply a decreased resolution in our final case with an increased keel depth to 1 m. By reducing the resolution, we are able to simulate a larger domain over a longer period of time (~1 hour versus 15 min) to see if results from the smaller keel simulations are applicable when ice accelerations are slower.

[41] Ice motion was gradually increased from a motionless initial state to a velocity of 0.43 m s^{-1} over the first hour of the simulation. An example of the resulting flow is presented in Figure 14, showing vertical cross sections taken after 70 and 90 min. As this figure shows, increasing the keel to a depth greater than the fresh layer thickness does not result in a complete blocking of the upstream fresh layer. Instead, the fresh layer tends to deepen upstream of the keel until it spills over, resulting in a strong transitional flow downstream from the keel, much like the 0.54-m keel simulation presented above. Water velocities immediately downstream from the keel (x = ~170 m) are nearly motionless, implying a large difference in ice/water velocity difference, approaching 0.43 m s^{-1}, between the ice surface and the first grid point below the ice. Downstream from the transition hydraulic jump, located at ~180 m at 70 min, the water velocities are more similar to the ice speed. As time progresses, the depth of the fresh layer increases so that by 90 min the hydraulic jump has moved closer to the keel. Lee-side velocities at this time have weakened, however, the wake region of the keel is still quite turbulent.

[42] The greater ice velocity and deeper keel in this case cause stronger turbulence activity downstream from the keel in comparison with the shallow-keel cases, as shown by a plane view plot of the cross-keel velocity component, u (Figure 15a). Near the keel, u is relatively smooth, with horizontal gradients that roughly follow the keel terrain. Downstream from the keel at about x = 170 m, the flow undergoes a hydraulic jump and becomes very turbulent, with rapid horizontal variations in the velocity. Horizontal variations in flow speed in this region show both a lee-side internal wave component, which varies in the downstream direction, and a cross-stream variation that is related to the ice depth gaps in the cross-flow direction. Notches in the keel tend to generate stronger downstream velocities as the stable layer is channeled by the keel geometry. Ice bottom heat fluxes (Figure 15b) corresponding to the horizontal velocity plot show how different scales of motion affect ice melt. In the lee transition region, we again see that strong near-surface flow generates a region of maximum heat flux related to high values of u_*. The jump region exhibits small-scale variability, suggesting that turbulence eddies are directly affecting the melting rates. Further downstream, maximum heat fluxes tend to follow the regions of stronger flow created by the keel notches. Adding to the melting heat flux variability is the freezing point depression (Figure 15c), which varies according to the vertical displacement of the fresh layer. The lee-side wake region and internal waves tend to generate areas with both high freezing point depression and large relative velocity (e.g., between x = 165 and 205 m). In contrast, low-velocity regions typically have lower salinity values, resulting in a smaller freezing point depression and reduced melting rates, for example, upstream from the keel and downstream from x = ~205 m. In general, model results suggest that freezing point depression has a significant effect on ice bottom melting rates, which are further enhanced in regions of high ice-relative water velocities.

4. Discussion and Conclusions

[43] A large-eddy simulation of the boundary layer under ice is performed, with an emphasis on understanding how keels affect the formation of turbulence and corresponding turbulent fluxes. Two scenarios are examined, the first focusing on the response of the boundary layer to a 10.8-m keel during winter conditions with a well-mixed boundary layer and a second concentrating on the very stable

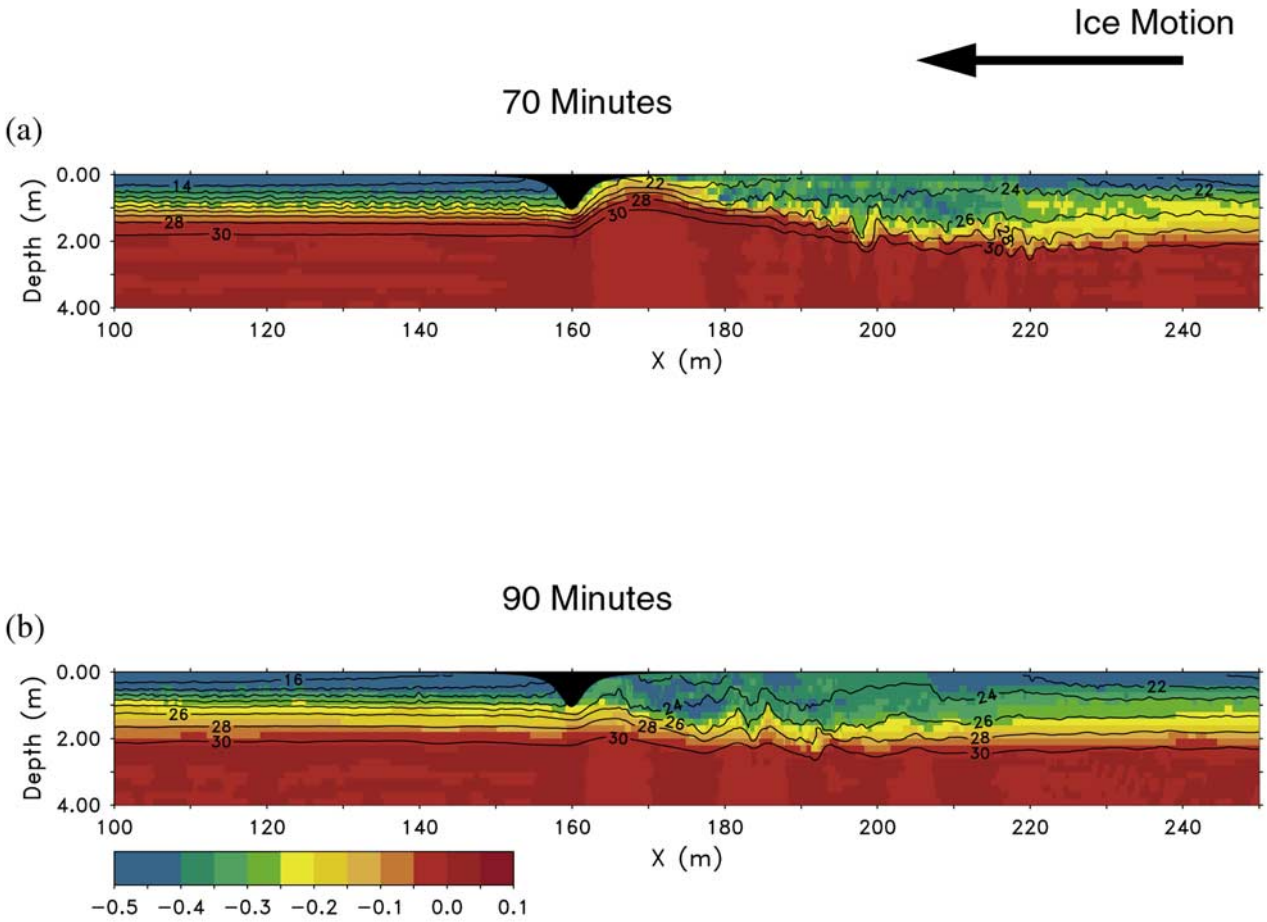

Figure 14. Vertical cross section from y = 6.3 m of the u velocity component (shaded, m s^{-1}) and salinity (contours, psu) for a keel height of 1.0 m after (a) 70 min and (b) 90 min.

conditions produced by ice melting in the summer. In both cases, the model is initialized at rest and forced by accelerating the surface ice to a velocity similar to observed ice motion during the SHEBA experiment. Heat and salinity fluxes between the ocean and ice are calculated using parameterized exchange rates based on the work of *McPhee et al.* [1987], which takes into account differences between the molecular diffusion of heat and salinity.

[44] For the wintertime keel problem, the LES model shows that flow over the keel generates a region of strong wake turbulence, with velocities in the lee of the keel adjusting to almost match the ice speed. Turbulent fluxes in the wake region are found to greatly exceed those produced in a simulation with a smaller keel depth of 1.8 m. In particular, we find that the keel generates a strong upward flux of heat from the underlying modified Atlantic water. This flux is produced by eddies that directly entrain warmer, more saline water from the pycnocline layer below 20-m depth. Flux calculations from the LES compare favorably with turbulent flux measurements made from a fixed mast during the SHEBA field program showing upward heat fluxes of ~25 W m^{-2} at 12-m depth. Our results also suggest that the angle of the flow relative to the keel has a significant impact on boundary layer fluxes. On the basis of these results, it is likely that the anomalous melting observed in March of the SHEBA experiment was due in part to increased entrainment heat fluxes forced by ice bottom keels.

[45] Results from the summertime case indicate that keels are very efficient at forcing turbulence in the fresh layer environment, causing enhanced local melting rates. Fresh water under the ice acts as an insulator as long as turbulent mixing is weak. This is because the fresh layer temperature approaches the local freezing point from heat lost as ice melts, ultimately limiting the melting rate of the ice. Water beneath the fresh layer is warmed by transmitted solar radiation mostly through leads and therefore has a temperature considerably higher than the local freezing point. If this water is transported vertically to the ice bottom through turbulence, then melting rates increase. Keels promote vertical turbulence transport and ice melting in three different ways. If the keel is deep enough, then it can penetrate into the saltier water that makes up the bulk of the remnant mixed layer from the previous cold season. As noted above, this water has a temperature above the local freezing point because of solar heating and will therefore melt ice more rapidly. The second way keels can enhance melting is by blocking the flow and causing an increase in the near-ice velocity over the keel. Increased velocity forces greater turbulence heat exchange and more rapid melting. Finally,

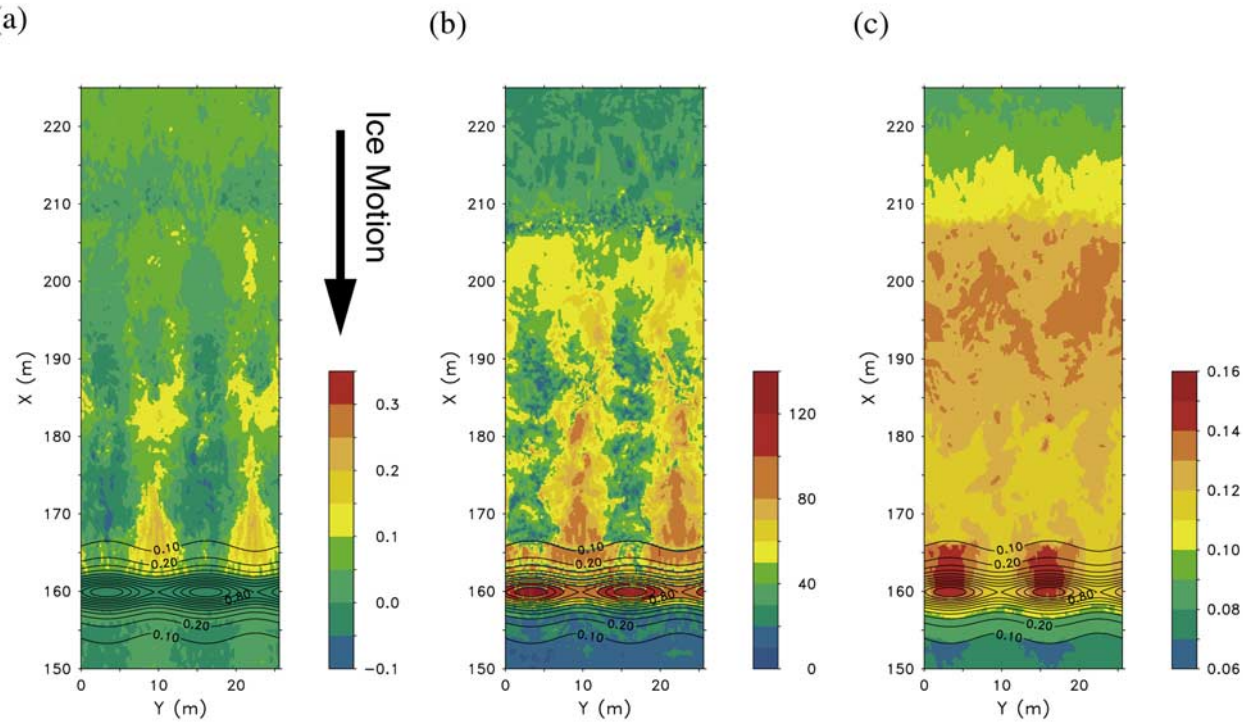

Figure 15. Horizontal cross sections of (a) u component of velocity (m s^{-1}) at 0.5-m depth, (b) ice bottom heat flux (W m^{-2}), and (c) ice bottom freezing point depression (°C) after 90 min. Also shown are contours of the keel depths in meters.

keels can force various internal wave modes in the stratified fresh layer, much like mountains affecting atmospheric flow. Strong lee-side currents and wave oscillations can transport fast moving, saltier water to the ice bottom, causing enhanced melting long distances downstream from the keel.

[46] Although keels tend to promote turbulence locally, keels can also ''inhibit'' total bottom ice melting by blocking the flow and effectively trapping fresh water upstream from the keel. In our simulations, we noted that keel turbulence typically decays as the fresh layer is blocked and accelerates to match the ice speed. The use of periodic boundaries emphasizes this effect in the model; however, actual ice conditions may have enough keels to allow for trapped fresh water, assuming the ice does not change shape through elastic processes (which was the case during SHEBA). Trapping of water by keels in a periodic domain can also be considered a simulation of a depression in the ice, for example, as produced by a frozen lead. Our results show that trapping probably hinders mixing of under-ice fresh water and should be considered in setting under-ice fluxes.

[47] In comparison with the summer fresh case, the effects of keels in the winter are less pronounced because neutral stability inhibits pressure drag across the keel, reducing the net drag of the ice bottom on the mixed layer. Even so, for the winter case we found that deep keels can generate enhanced entrainment of heat and salinity into the mixed layer, lowering the freezing point and causing ice bottom melting when the upward ice heat conduction was small.

[48] Our results provide only a glimpse of the turbulent processes that are active around ice keels. In general, we find that keels promote greater mixing, but also can create regions of trapped water when the water is stratified, which decreases ice bottom fluxes. In most cases, if we compare flux values without keels to the cases presented here, we find that keels greatly increase the strength of turbulent fluxes. For example, in the wintertime case where we have turbulent flux data, our results suggest that keels could be responsible for much of the vertical heat exchange between the boundary layer and the deeper ocean. In the summer, stratification complicates our understanding of how the under-ice boundary layer behaves. Our simulations show both increased fluxes near the keel and lower fluxes where water is trapped. Generalizing these results is not easy without knowing the under-ice structure and the time history of the ice velocity. However, we can conclude that hydraulic flow parameters, such as the Froude number, provide a measure of flow stability, indicating that mean flow parameters and keel dimensions could be used to estimate mixing rates.

[49] Current parameterizations of ice bottom fluxes in ocean general circulation models are typically based on simple approximations, for example, by assuming a wall layer structure where fluxes are a function of the ice/water velocity differential and an ice bottom roughness length [*Holland et al.*, 1997]. The hope in using these approaches is that complicated flow structure, as shown in our simulations, can be accounted for by averaging. In cases with relatively uniform ice features and weak stratification, this assumption may be sufficient. However, as our results show,

the presence of keels and stratification can have a large impact on ice bottom fluxes, especially during the summer melt season when the upper ocean is strongly stratified.

[50] Contemporary ice models [e.g., *Schramm et al.*, 2000; *Holland et al.*, 1997; *Bitz et al.*, 2001] have begun to treat sea ice using a range of ice parameters, including ice classes that permit ridging and lead physics. For example, *Holland et al.* [1997] approximate increased mixing from keels by using a higher u_* for ice greater that 3 m in thickness. Although keels and ridges have not been specifically addressed in these models, the problem is recognized and will be addressed in future developments. For example, the next generation of ice models should take into consideration both variations in the ice bottom roughness and pressure drag effects associated with keels that do not fit the usual similarity approach. Ice parameterizations also need to be modified to include thin fresh layers that cannot be resolved by ocean general circulation models (OGCMs). These layers could be addressed using a bulk layer model, with exchange between the fresh layer and ocean boundary layer controlled by an entrainment rate that is a function of ice motion, keel characteristics, and average Froude number values. More extensive observations combined with LES experiments representing a range of keel depths could be used as a first cut data set for determining fresh water entrainment rates in the summer and mixed-layer fluxes in the well-mixed wintertime boundary layer.

[51] Including all of the effects examined here in an ice-turbulent flux parameterization is a daunting task. However, we note that during SHEBA the strong fresh layer effects were probably limited to only a short period of time at the end of July when the ice begin moving and breaking apart. During this time, the fresh layer was rapidly mixed with the rest of the boundary layer, resulting in a mixed layer more in line with typical boundary layer parameterization assumptions. Still, the effects of deep keels on turbulence transport need to be accounted for, particularly with respect to enhanced entrainment at the mixed-layer base. The conditions observed during SHEBA are likely to be unrepresentative of all years. Previous long-term field experiments [*Nansen*, 1902] indicate that the summer fresh layer is not always destroyed at the end of the melt season but can be refrozen in the fall before mixing with the rest of the boundary layer. Under such conditions, more modest ice motion could cause enhanced ice melting that would vary with ice speed and the ice bottom characteristics.

[52] **Acknowledgments.** We thank Hajo Eichen and two anonymous reviewers for their very helpful suggestions. We also would like to acknowledge the supercomputer time provided by the National Center for Atmospheric Research, which is funded by the National Science Foundation. This work was supported as part of the Surface Heat Budget of the Arctic (SHEBA) project by National Science Foundation grants OCE-97-03539, OPP-00-84284, and the Office of Naval Research grant N00014-01-1-0022/ORSC.

References

Baines, P. G., *Topographic Effects in Stratified Flows*, 482 pp., Cambridge Univ. Press, New York, 1995.

Baines, P. G., and K. P. Hoinka, Stratified flow over two-dimensional topography in fluid of infinite depth: A laboratory simulation, *J. Atmos. Sci.*, *42*, 1614–1630, 1985.

Bitz, C. M., M. M. Holland, A. J. Weaver, and M. Eby, Simulating the ice-thickness distribution in a coupled climate model, *J. Geophys. Res.*, *106*, 2441–2464, 2001.

Denbo, D. W., and E. D. Skyllingstad, An ocean large eddy simulation model with application to deep convection in the Greenland Sea, *J. Geophys. Res.*, *101*, 1095–1110, 1996.

Gallus, W. A., and J. B. Klemp, Behavior of flow over step orography, *Mon. Weather Rev.*, *128*, 1153–1176, 2000.

Holland, M. M., J. A. Curry, and J. L. Schramm, Modeling the thermodynamics of a sea ice thickness distribution, 2, Sea ice/ocean interaction, *J. Geophys. Res.*, *102*, 23,093–23,108, 1997.

Long, R. R., Some aspects of the flow of stratified fluids, III, Continuous density gradients, *Tellus*, *7*, 341–357, 1955.

Maykut, G. A., Energy exchange over young sea ice in the central Arctic, *J. Geophys. Res.*, *83*, 3646–3658, 1978.

McPhee, M. G., Turbulent stress at the ice/ocean interface and bottom surface hydraulic roughness during the SHEBA drift, *J. Geophys. Res.*, *107*(C10), 8037, doi:10.1029/2001JC000633, 2002.

McPhee, M. G., G. A. Maykut, and J. H. Morison, Dynamics and thermodynamics of the ice/upper ocean system in the marginal ice zone of the Greenland Sea, *J. Geophys. Res.*, *92*, 7017–7031, 1987.

Nansen, F., *The Norwegian North Polar Expedition 1893–1896 Scientific Results*, vol. 5, Jacob Dybwad, Christiana, 1902.

Perovich, D. K., and B. Elder, Estimates of ocean heat flux at SHEBA, *Geophys. Res. Lett.*, *29*(10), 1344, doi:10.1029/2001GL014171, 2002.

Perovich, D. K., T. C. Grenfell, J. A. Richter-Menge, B. Light, W. B. Tucker, and H. Eicken, Thin and thinner: Ice mass balance measurements during SHEBA, *J. Geophys. Res.*, *108*(C3), 8050, doi:10.1029/2001JC001079, 2003.

Rigby, F. A., and A. Hanson, Evolution of a large Arctic pressure ridge, *AIDJEX Bull.*, *34*, 43–71, 1976.

Schramm, J. L., G. M. Flato, and J. A. Curry, Toward the modeling of enhanced basal melting in ridge keels, *J. Geophys. Res.*, *105*, 14,081–14,092, 2000.

Skyllingstad, E. D., and D. W. Denbo, Large eddy simulation of turbulence under sea ice and leads, *J. Geophys. Res.*, *106*, 2477–2498, 2001.

Skyllingstad, E. D., and H. W. Wijesekera, Large-eddy simulation of flow over obstacles: High drag states and mixing, *J. Phys. Oceanogr.*, in press, 2003.

Tripoli, G. J., A nonhydrostatic mesoscale model designed to simulate scale interaction, *Mon. Weather Rev.*, *120*, 1342–1359, 1992.

Wadhams, P., Sea ice thickness distribution in the Greenland Sea and Eurasian Basin, May 1987, *J. Geophys. Res.*, *97*, 5331–5348, 1992.

M. G. McPhee, McPhee Research Company, 450 Springs Road, Naches, WA 98937, USA.

C. A. Paulson, W. S. Pegau, and E. D. Skyllingstad, College of Oceanic and Atmospheric Sciences, Oregon State University, 104 Ocean Administration Building, Corvallis, OR 97331, USA. (skylling@oce.orst.edu)

T. Stanton, Naval Postgraduate School, Monterey, CA 93943, USA.